DOI: 10.1002/((please add manuscript number))
Article type: Communication

Scalable Polymer Nanocomposites with Record High-Temperature Capacitive Performance Enabled by Rationally Designed Nanostructured Inorganic Fillers

*He Li, Ding Ai, Lulu Ren, Bin Yao, Zhubing Han, Zhonghui Shen, Jianjun Wang, Long-Qing Chen and Qing Wang**

H. Li, D. Ai, L. Ren, B. Yao, Z. Han, Z. Shen, Dr. J. Wang, Prof. L.-Q. Chen, Prof. Q. Wang
Department of Materials Science and Engineering, The Pennsylvania State University, University Park, Pennsylvania 16802, USA
E-mail: wang@matse.psu.edu

Keywords: polymer nanocomposites, nanostructured fillers, capacitors, high temperature, energy density

Abstract: Next-generation microelectronics and electrical power systems call for high-energy-density dielectric polymeric materials that can operate efficiently under elevated temperatures. However, the currently available polymer dielectrics are limited to relatively low working temperatures. Here, we report the solution-processable polymer nanocomposites consisting of readily prepared Al_2O_3 fillers with systematically varied morphologies including nanoparticles, nanowires and nanoplates. The field-dependent electrical conduction of the polymer nanocomposites at elevated temperatures has been investigated. A strong dependence of the conduction behavior and breakdown strength of the polymer composites on the filler morphology has been revealed experimentally and further rationalized via computations. The polymer composites containing Al_2O_3 nanoplates display the record capacitive performance, *e.g.* a discharged energy density of 3.31 J/cm^3 and a charge-discharge efficiency of >90% measured at 450 MV/m and 150 ^oC, significantly outperforming the state-of-the-art dielectric polymers and nanocomposites that are typically prepared via tedious, low-yield approaches.

Dielectric film capacitors have the highest power density (on the order of MW) and the best rate capability (on the order of μs) among the electrical energy storage devices and are the key components in advanced electronics and electrical power systems.[1,2] Polymer dielectrics are enabling materials for high-energy-density film capacitors owing to their unique features such as facile processability, high breakdown strength and great reliability under the applied electric fields.[3-12] For instance, biaxially oriented polypropylene (BOPP) is currently used in the power inverters of electric vehicles to control and convert direct current from batteries into alternating current required to drive the motor. Nevertheless, polymer dielectrics suffer from relatively low working temperatures, and thus fall far short of the increasing demands on electrical energy storage and conversion under extreme conditions often found in transportation, aerospace power systems and microelectronics.[13] BOPP can operate only at temperatures below 105 ºC due to exponential increases of conduction loss and sharp decreases of the breakdown strength with increasing temperature.[14,15] To accommodate BOPP film capacitors in electric vehicles, an additional radiator system is applied onto the power inverters to decrease the environmental temperature from ~140 to ~70 ºC.[15] This unfortunately increases the complexity of the integrated power system and concurrently decreases fuel efficiency. In power electronics, emerging wide bandgap semiconductors, *e.g.* silicon carbide and gallium nitride, which hold the potential to revolutionize electronics, necessitate the next-generation capacitors with operating temperatures >150 ºC.[16] Although a number of engineering polymers have been exploited as dielectric materials for elevated temperature applications, this approach has met with limited success.[17-22]

More recently, the dielectric polymer composites have been prepared via incorpoartion of hexagonal boron nitride nanosheets (BNNSs) into the polymer matrix.[23,24] It has been demonstrated that the introduced BNNSs significantly suppresses electrical conduction and hence leads to the polymer composites with outstanding high-temperature energy storage and discharging properties. However, BNNSs are typically prepared by liquid phase exfoliation from the powders;[25,26] this is a time-consuming (*i.e.* ~48 hrs) and low-yield (e.g. less than 10%) technique and thereby severely

hinders the scaling up of this approach. Herein we report the scalable polymer nanocomposites consisting of nanostructured γ-Al_2O_3 fillers that are readily prepared by well-eatablished hydrothermal synthesis[27]. The effect of the nanofiller morphology on the electrical energy storage properties of the composites and the field-dependent electrical conduction bahavior at various temperatures have been uncovered. Excellent capacitive performance that exceeds all the current dielectric polymers and composites has been demonstrated in the Al_2O_3 nanoplate-based polymer nanocomposites at elevated temperatures.

Compared to BNNSs, γ-Al_2O_3 has a larger band gap (7.2~8.8 eV *vs.* ~5.97 eV) and a much greater dielectric constant (*K*, 9~10 *vs.* 3~4), along with a high dielectric breakdown strength of 600-800 MV/m,[28,29] making it an ideal filler platform for high-temperature dielectric polymer composites possessing high energy densities and low losses. The energy denisty of dielectric materials is proportional to its *K*, while a large bandgap would help to reduce the conduction loss, which is the main loss mechanism of dielectric materials operating at elevated temperatures and high electric fields.[14,18] Al_2O_3 nanofillers have been utilized to enhance *K* and reduce leakage current of polymer composites at ambient temperature.[30,31] As shown in Figure S1, Supporting Information, divinyltetramethyldisiloxane-bis(benzocyclobutene) (BCB) was thermally cross-linked in the presence of the γ-Al_2O_3 nanostructures including nanoparticles (NPs, an average diameter of 20 nm), nanowires (NWs, an average length of 80 nm and a mean diameter of 5 nm) and nanoplates (NPLs, an average thickness of 30 nm and a width of 800-1000 nm in hexagonal shape) (Figure S2, Supporting Information) to afford the respective composite *c*-BCB/Al_2O_3-NPs, *c*-BCB/Al_2O_3-NWs and *c*-BCB/Al_2O_3-NPLs films with a thickness of 12 ± 2 μm (Figure S3, Supporting Information). The γ phase of Al_2O_3 fillers is verified by the existence of the face-centered cubic (fcc) structure in the X-ray diffraction patterns (Figure S4, Supporting Information). The dielectric spectra of *c*-BCB/Al_2O_3 nanocomposites are presented in Figures S5-S8, Supporting Information. **Figure 1**a reveals the apparent increase of *K* of the composites with increasing filler content, *e.g.* from 2.81 of the neat *c*-BCB to 3.62 of *c*-BCB/Al_2O_3-NPs, 3.81 of *c*-BCB/Al_2O_3-NWs and 3.8 of *c*-BCB/Al_2O_3-

NPLs with 10.5 vol% fillers meausured at room temperature and 1 kHz. Comparatively, *K* of *c*-BCB/10 vol% BNNSs is around 3.09. As expected, the NW and NPL fillers give rise to higher *K* of the composites relative to the polymer filled with the same content of the Al_2O_3 NPs, which is attributable to their larger dipole moments as a result of higher aspect ratios of NWs and NPLs.[32] The variations of effective *K* with the filler content are fitted fairly well by using the Parallel mixing model for the NP-based composites and Polder-Van Santen (PVS) formalism for the polymer composites with NW and NPL fillers.[32,33] It is known that the interfacial effect also contributes to the polarizability and *K* of the composites.[34] As the surface area of NPLs, *i.e.* ~18 m^2/g, is much smaller than that of NWs, *i.e.* ~210 m^2/g, there exists a small difference in *K* vales of the composites despite of a likely higher *K* of NPLs. At relatively high contents of the fillers (*e.g.* > 9 vol%), *K* of the NW-composite even surpasses that of the composite with NPLs, further evidencing the role of the interfacial effect in the composites. Different from *c*-BCB/BNNSs, the weak-field dielectric loss increases slightly with the incorporation of Al_2O_3 fillers into *c*-BCB (Figure 1a) owing to the contribution of the polar group, such as -OH, from alumina to the relaxation loss. As presented in Figure 1b, the dielectric properties of *c*-BCB/Al_2O_3 were found to remain almost constant over a wide temperature range of 25 - 200 ^oC and in the frequency range of 100 Hz to 1 MHz measured at 150 ^oC.

The breakdown strength of the dielectric films was analyzed and shown in Figures S9-S10, Supporting Information, according to two-parameter Weibull statistic,[35]

$$P(E) = 1 - \exp(-(E/E_b)^{\beta}) \quad \text{(Eq. 1)}$$

where *P(E)* is the cumulative probability of electric failure, *E* is the measured breakdown field, E_b is the characteristic breakdown strength which corresponds to a ~63% probability of failure, and the shape parameter β evaluates the scatter of data. **Figure 2**a plots the E_b of the dielectric films measured at 150 ^oC. Clearly, the addition of Al_2O_3 significantly enhances E_b, *e.g.* from 284 MV/m of unfilled *c*-BCB to 334 MV/m of *c*-BCB/Al_2O_3-1.5 vol% NPs, 385 MV/m of *c*-BCB/Al_2O_3-3

vol% NWs and 489 MV/m of *c*-BCB/Al_2O_3-7.5 vol% NPLs. Notably, E_b of *c*-BCB/Al_2O_3-7.5 vol% NPLs is even greater than that of the state-of-the-art high-temperature composite *c*-BCB/BNNSs (*i.e.* 421 MV/m)[23]. Impressively, the Al_2O_3-based polymer composites show excellent stability of E_b with respect to temperature as displayed in Figure 2b. For example, when temperature increases from 25 ^oC to 200 ^oC, E_b of *c*-BCB/Al_2O_3-7.5 vol% NPLs is reduced by merely 3.6%, *i.e.* from 500 to 482 MV/m in comparison to 6.9% change of E_b of *c*-BCB/BNNSs, *i.e.* from 447 to 416 MV/m. By contrast, E_b of polyetherimide (PEI), which is among the best high-temperature dielectric polymers, falls steeply with rising temperature, *e.g.* from 501 MV/m at 25 ^oC to less than 400 MV/m at 200 ^oC. The cross-linking of BCB in the presence of the fillers improves interfacial compatibility of the fillers and polymer matrix and reduces the probability of the formation of interfacial defects, thus contributing to the improvement in E_b. The further addition of the Al_2O_3 fillers into *c*-BCB leads to the reduction in E_b, which is attributed to filler aggregation as evidenced by the decrease in the Young's modulus (Figure S11, Supporting Information), the increase in the conduction current (see the discussion below) and electron microscopic images (Figure S12, Supporting Information).

The monotonic and pronounced increase in E_b from the NP-, NW- to NPL-containing composites has been understood by using the continuum phase-field model.[36,37] As illustrated in Figure 2c, the NPLs provide high resistance to the dendrite growth of the breakdown phase, whereas it is much easier for the crack to penetrate or get around NPs, thus yielding the lowest E_b of the composites loaded with NPs when compared to the NW- and NPL-based composites. The simulated evolution of the breakdown phase is quantitatively displayed in Figure S13, Supporting Information. It can be seen that the predicted breakdown strengthes are maximized at around 310 MV/m, 390 MV/m and 480 MV/m for the polymer composites with NPs, NWs and NPLs, respectively, which are in excellent agreement with the experimental results. The enhancement in E_b of the polymer composites can be further understood from the simulated electric feld distribution

in the composites, as depicted in Figure 2d. Apparently, the parallel NPLs are the most effective in dispersing the applied electric field throughout the polymer matrix to mitigate the inhomogeneous distribution of local electric fields. For the composites with NPs and NWs, the electric fields are highly concentrated around the NPs and at the vertices of the NWs, respectively, in the composites, which leads to the easy formation of breakdown paths, and consequently, compromised E_b and increased leakage current (see the discussion below).[37]

Figure S14 (Supporting Information) presents the electric displacement-electric field (*D*-*E*) loops of the polymer nanocomposites measured at 250 MV/m and 150 °C. Consistent with the trend observed for the weak-field *K* values, there evidently exists a systematic increase in the maximum value of *D* of the composites, *e.g.* from 0.698 μC/cm^2 of *c*-BCB to 0.975 μC/cm^2 with adding 10.5 vol% NPLs, which is greater than that of *c*-BCB/BNNSs (*i.e.* 0.768 μC/cm^2). Accordingly, the polymer nanocomposite with 7.5 vol% Al_2O_3 NPLs displays higher stored energy density (U_s) than 10 vol% BNNSs at elevated temperatures (Figure S15, Supporting Information). For practical capacitor applications, in addition to enhancing energy density, minimizing the dielectric loss, especially the loss at high electric fields, is equally important. Furthermore, at elevated tempeartures, the loss becomes more significant owing to thermally-assisted tunneling effect and other conduction mechanisms.[14] For instance, while BOPP shows a negligible loss of less than 0.05% at 1 kHz in the room-temperature dielectric spectrum, the loss rises exponentially to 29.8% when an electric field of 400 MV/m is applied and operation temperature increases to 120 °C.[35] The loss not only leads to reduced discharged energy density (U_e) and lowered charge-discharge efficinecy ($\eta = U_e/U_s \times 100\%$) but also generates Ohmic heat to endanger the reliability and lifetime of dielectric polymers. As shown in Figure S16, Supporting Information, *c*-BCB/Al_2O_3-NPLs possesses the best U_e and η, or equivalently the lowest loss, at high electric fields and elevated temperatures when compared to the respective Al_2O_3 NW- and NP-containing composites. Particularly, *c*-BCB/Al_2O_3-NPLs outperforms the current high-temperature dielectric polymers, including PEI, fluorene polyester (FPE), and polyimide (Kapton® PI), and *c*-BCB/BNNSs, as summarized in **Figure 3**. At 150 °C, *c*-

BCB/Al_2O_3-7.5 vol% NPLs delivers an U_e of 4.07 J/cm^3 *vs.* 2.42 J/cm^3 of *c*-BCB/BNNSs and ~1.6 J/cm^3 of PEI. Impressively, *c*-BCB/Al_2O_3-7.5 vol% NPLs maintains a η of >90% even at 450 MV/m, which is unattainable in the currently available dielectric polymers and composites. As compared in Figure S17 Supporting Information, under the same applied field, η of BOPP is ~83.5% at 100 ^{o}C and ~61.8% at 120 ^{o}C.[38] Very recently, the BNNS and SiO_2 layers have been surface-coated onto the polymer films to block charge injection from the electrodes and reduce high-field conduction loss at elevated temperatures.[38,39] The BNNS- and SiO_2-functionalized PEI films exhibit η of 77.4% and 85.1%, respectively, at 450 MV/m and 150 ^{o}C. Additionally, the maximum U_e values at η > 90% of the BNNS-and SiO_2-coated PEI and *c*-BCB/BNNSs are also much inferior to that of *c*-BCB/Al_2O_3-NPLs (Figure 17b, Supporting Information). At 200 ^{o}C, the polymer composite with 7.5 vol% Al_2O_3 NPLs exhibits an U_e of 3.02 J/cm^3 and a η of 76.1% at 450 MV/m, far exceeding those have been achieved in the dielectric polymers and polymer nanocomposites.[18,21]

Electrical conduction is the well-recognized dominant loss mechanism of dielectric materials operating at high fields.[14,23,40] Understanding of the impact of the filler on field- and temperature-dependent electrical conduction is therefore vital in order to provide insights into the high-temperature capacitive results of the composites. As shown in **Figure 4**a, the introduction of the Al_2O_3 fillers leads to a dramatic decrease in the current density (J) at high electric fields and elevated temperatures, *e.g.* from 5.5×10^{-8} A/cm^2 of *c*-BCB to 1.12×10^{-9} A/cm^2 of *c*-BCB/Al_2O_3-7.5 vol% NPLs measured at 200 MV/m and 150 ^{o}C. Of particular to note that J of *c*-BCB/Al_2O_3-7.5 vol% NPLs is lower than those of 7.5 vol% Al_2O_3-NPs and -NWs filled *c*-BCB composites as well as *c*-BCB/BNNSs (*i.e.* 1.85×10^{-9} A/cm^2) and the high-temperature dielectric polymers (Figure S18 Supporting Information). The superior electrical resistivity of the composites and the highest electrical resistivity of *c*-BCB/Al_2O_3-NPLs thus accounts for the much reduced high-field dielectric loss and associated enhancement in η and U_e observed in the composites and elucidates the best

capacitive performance of the Al_2O_3 NPL-based composite, respectively. The opposite tendency between the loss determined from the *D-E* loops (Figure S19, Supporting Information) and that measured from dielectric spectroscopy (Figure 1a) with respect to the content of Al_2O_3 fillers in the polymer reaffirms different origins of the loss observed at weak- and high-fields. Interestingly, it is evident that Al_2O_3 is more efficient in impeding electrical conduction under the condition of high electric fields and elevated temperatures. For instance, at an applied field of 150 MV/m, the leakage current measured at 25 °C is reduced by 86% with adding 7.5 vol% Al_2O_3 NPLs into *c*-BCB. This reduction in the current increases to 97% when temperature rises to 150 °C (Figure S20, Supporting Information).

As shown in Figure 4a and Figure S21, Supporting information, *J* has been measured as a function of applied fields and temperatures. The threshold field (E_{thr}), where the slope of the conduction current changes with the applied field, depends on both the spatial distribution and the depth of trapping sites. E_{thr} is related to the activation energy (W_a) according to Equation 2 (ref. 41)

$$E_{thr} \sim \exp(W_a / K_B T) \quad \text{(Eq. 2)}$$

where K_B is the Boltzmann constant. E_{thr} of *c*-BCB and *c*-BCB/Al_2O_3 decreases steadily with the increase of temperature, denoting lower W_a at high temperatures. It can be inferred that E_{thr} corresponds to the critical electric field required for transition of the conduction mechanism from Ohmic to non-Ohmic behavior in the films. According to the hopping conduction equation,[42,43] *J* is given as,

$$J(E,T) = 2ne\lambda v * \exp(-W_a / K_B T) * \sinh(\lambda eE / 2K_B T) \quad \text{(Eq. 3)}$$

$$J(E) = A * \sinh(B * E) \quad \text{(Eq. 4)}$$

where *n* is the carrier concentration, λ is the hopping distance, *v* is the attempt-to-escape frequency, W_a is the activation energy in eV, *e* is the charge of the carriers, *m* is the mass of the free electron. The curve fits of Equation 3 to hyperbolic sine are presented in Figure 4c, which fit well with the experimental data with quality of fitting, R^2, ranging from 0.966 to 0.997. This is a strong indication

that hopping is the major conduction mechanism in *c*-BCB and the composite at 150 °C. Fitting the *J-E* data to the hopping conduction model gives a hopping distance, which increases from 1.22 nm to 1.94 nm in pristine *c*-BCB and from 0.7 nm to 1.36 nm in *c*-BCB/Al_2O_3-NPLs as temperature increases from 100 to 250 °C. As can be seen in Figure 4d, E_{thr} of *c*-BCB/Al_2O_3-NPLs is always higher than that of *c*-BCB, indicative of higher W_a and shorter hopping distances of the composite. As a shorter hopping distance corresponds to a deeper trap depth,[44] the increased trap depth caused by the Al_2O_3 NPL fillers, is thus responsible for the large drop in the leakage current and dielectric loss, as well as the great improvements in η and U_e observed in the composite. In addition, E_{thr} of *c*-BCB/Al_2O_3-NPLs is higher than the respective composites loaded with Al_2O_3 NWs and NPs, clearly manifesting its highest W_a calculated from Arrhenius equation (A_a) (Figure S22, Supporting Information), the shortest hopping distance and the deepest trap depths induced by NPLs relative to those from NWs and NPs (Figure 4b). This correlates well with the characterization results of electrical conduction and capacitive performance. The hopping distances of the nanocomposites with varied contents of the Al_2O_3 nanofillers were calculated (Figure S23, Supporting Information) and summarized in Table S4, Supporting Information. It is found that the hopping distance decreases initially and then increases with the increase of filler content, indicating that there exists a threshold concentration of the nanofiller beyond which the suppression of the conduction current becomes less effective. The increased shallow traps at high loadings of the nanofiller are likely traced to the filler agglomeration, which behave as conducting paths and result in high conduction current.

In summary, we have successfully demonstrated that addition of nanostructured Al_2O_3 introduces deep traps in the polymer matrix and significantly reduces conduction current especially at high applied fields and elevated temperatures. The synergistic features, including a wide bandgap in conjunction with a relatively high dielectric constant, of Al_2O_3 furnish the resulting polymer composites with comprehensive advantages, including high U_e, great η, remarkable E_b and excellent dielectric stability at high applied fields and elevated temperatures, which represent a

marked improvement over the current high-temperature dielectric polymers and composites. Furthermore, the systematic manipulation of the morphology of the nanofillers from NPs, NWs to NPLs has been specifically exploited to further boost the elevated-temperature capacitive performance of the polymer composites. This facile approach sheds light on the rational design of scalable high-performance high-temperature dielectric polymer composites and reveals great potential for the practical use of dielectric polymeric materials in power electronics and electrical systems under extreme environments.

Supporting Information
Supporting Information is available from the Wiley Online Library or from the author.

Acknowledgements
The authors acknowledge the support from the US Office of Naval Research.

Received: ((will be filled in by the editorial staff))
Revised: ((will be filled in by the editorial staff))
Published online: ((will be filled in by the editorial staff))

References

[1] W. J. Sarjeant, I. W. Clelland, R. A. Price, *Proc. IEEE* **2001**, *89*, 846.

[2] Q. Tan, P. Irwin, Y. Cao, *IEEJ Trans. Fund. Mater.* **2006**, *126*, 1152.

[3] C. W. Nan, Y. Shen, J. Ma, *Annu. Rev. Mater. Res.* **2010**, *40*, 131.

[4] Z. M. Dang, J. K. Yuan, S. H. Yao, R. J. Liao, *Adv. Mater.* **2013**, *25*, 6334.

[5] B. Chu, X. Zhou, K. Ren, B. Neese, M. Lin, Q. Wang, F. Bauer, Q. M. Zhang, *Science* **2006**, *313*, 334.

[6] L. Zhu, *J. Phys. Chem. Lett.* **2014**, *5*, 3677.

[7] Y. Wang, J. Cui, L. Wang, Q. Yuan, Y. Niu, J. Chen, Q. Wang, H. Wang, *J. Mater. Chem. A* **2017**, *5*, 10849.

[8] S. Luo, J. Yu, S. Yu, R. Sun, L. Cao, W. H. Liao, C. P. Wong, *Adv. Energy Mater.* **2019**, *9*,

1803204.

[9] X. Huang, P. Jiang, *Adv. Mater.* **2015**, *27*, 546.

[10] Z. Pan, L. Yao, J. Zhai, X. Yao, H. Chen, *Adv. Mater.* **2018**, *30*, 1705662.

[11] H. Li, F. Liu, B. Fan, D. Ai, Z. Peng, Q. Wang, *Small Methods* **2018**, *2*, 1700399.

[12] Y. Qiao, M. S. Islam, K. Han, E. Leonhardt, J. Zhang, Q. Wang, H. J. Ploehn, C. Tang, *Adv. Funct. Mater.* **2013**, *23*, 5638.

[13] R. W. Johnson, J. L. Evans, P. Jacobsen, J. R. Thompson, M. Christopher, *IEEE Trans. Electron. Packag. Manuf.* **2004**, *27*, 164.

[14] J. S. Ho, T. R. Jow, *IEEE Trans. Dielect. Elect. Insul.* **2012**, *19*, 990.

[15] M. Rabuffi, G. Picci, *IEEE Trans. Plasma Sci.* **2002**, *30*, 1939.

[16] J. Watson, G. Castro, *Analog Dialogue* **2012**, *46*, 1.

[17] D. Tan, L. L. Zhang, Q. Chen, P. Irwin, *J. Electron. Mater.* **2014**, *43*, 4569.

[18] Q. Li, F. Z Yao, Y. Liu, G. Zhang, H. Wang, Q. Wang, *Annu. Rev. Mater. Res.* **2018**, *48*, 219.

[19] J. Pan, K. Li, S. Chuayprakong, T. Hsu, Q. Wang, *ACS Appl. Mater. Inter.* **2010**, *2*, 1286.

[20] J. Pan, K. Li, J. Li, T. Hsu, Q. Wang, *Appl. Phys. Lett.* **2009**, *95*, 022902.

[21] J. S. Ho, S. G. Greenbaum, *ACS Appl. Mater. Interfaces*, **2018**, *10*, 29189.

[22] Z. Zhang, D. H. Wang, M. H. Litt, L. S. Tan, L. Zhu, *Angew. Chem. Int. Ed.* **2018**, *57*, 1528.

[23] Q. Li, L. Chen, M. R. Gadinski, S. Zhang, G. Zhang, H. U. Li, E. Iagodkine, A. Haque, L. Q. Chen, T. N. Jackson, Q. Wang, *Nature* **2015**, *523*, 576.

[24] Q. Li, F. Liu, T. Yang, M. R. Gadinski, G. Zhang, L. Q. Chen, Q. Wang, *Proc. Natl. Acad. Sci. USA* **2016**, *113*, 9995.

[25] J. N. Coleman, et al. *Science*, **2011**, *331*, 568.

[26] T. Morishita, H. Okamoto, Y. Katagiri, M. Matsushita, K. Fukumori, *Chem. Commun.* **2015** *51*, 12068.

[27] C. Kaya, J. Y. He, X. Gu, E. G. Butler, *Micropor. Mesopor. Mater.* **2002**, *54*, 37.

[28] S. Toyoda, T. Shinohara, H. Kumigashira, M. Oshima, Y. Kato, *Appl. Phys. Lett.* **2012**, *101*, 231607.

[29] Y. S. Min, Y. J. Cho, C. S. Hwang, *Chem. Mater.* **2005**, *17*, 626.

[30] Y. Thakur, M. H. Lean, Q. M. Zhang, *Appl. Phys. Lett.* **2017**, *110*, 122905.

[31] Z. Pan, L. Yao, J. Zhai, B. Shen, S. Liu, H. Wang, J. Liu, *J. Mater. Chem. A* **2016**, *4*, 13259.

[32] G. Zhang, X. Zhang, T. Yang, Q. Li, L. Q. Chen, S. Jiang, Q. Wang, *ACS Nano* **2015**, *9*, 7164.

[33] N. Guo, S. A. DiBenedetto, P. Tewari, M. T. Lanagan, M. A. Ratner, T. J. Marks, *Chem. Mater.* **2010**, *22*, 1567.

[34] T. J. Lewis, *J. Phys. D: Appl. Phys.* **2005**, *38*, 202.

[35] L. A. Dissado, J. C. Fothergill, S. V. Wolfe, R. M. Hill, *IEEE Tran. Electr. Insul.* **1984**, EI-*19*, 227.

[36] Z. H. Shen, J. J. Wang, Y. H. Lin, C. W. Nan, L. Q. Chen, Y. Shen, *Adv. Mater.* **2018**, *30*, 1704380.

[37] Z. H. Shen, J. J. Wang, J. Y. Jiang, Y. H. Lin, C. W. Nan, L. Q. Chen, Y. Shen, *Adv. Energy Mater.* **2018**, *8*, 1800509.

[38] Y. Zhou, Q. Li, B. Dang, Y. Yang, T. Shao, H. Li, J. Hu, R. Zeng, J. He, Q. Wang, *Adv. Mater.* **2018**, *30*, 1805672.

[39] A. Azizi, M. R. Gadinski, Q. Li, M. A. AlSaud, J. Wang, Y. Wang, B. Wang, F. Liu, L. Q. Chen, N. Alem, Q. Wang, *Adv. Mater.* **2017**, *29*, 1701864.

[40] Q. Burlingame, S. Wu, M. Lin, Q. M. Zhang, *Adv. Energy Mater.* **2013**, *3*, 1051.

[41] J. Beyer, P. H. F. Morshuis, J. J. Smit, *Conf. Electr. Insul. Dielectr. Phenomena*, IEEE, Victoria BC, Canada **2000**, *2*, 617.

[42] K. C. Kao, *Dielectric Phenomena in Solids* (Elsevier Academic Press, San Diego) **2004**, pg. 381.

[43] V. Ambegaokar, B. I. Halperin, J. S. Langer, *Phys. Rev. B* **1971**, *48*, 2612.

[44] Y. Yin, X. Dong, J. Chen, Z. Li, Z. M. Dang, *IEEJ Trans. Funda. Mater.* **2006**, *126*, 1064.

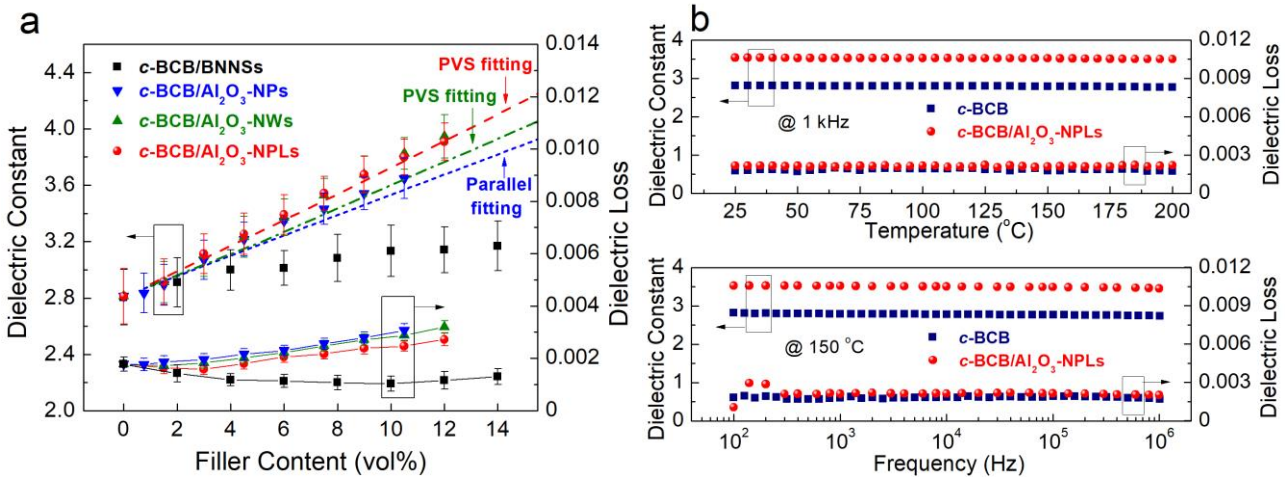

Figure 1. a) Dielectric constant and loss of the composites as a function of filler content measured at room temperature and 1 kHz. The dot lines respresent the theoretical fit of the effective dielectric constants of the composites. **b)** (top) Temperature- and (bottom) frequency-dependent dielectric spectra of *c*-BCB and the *c*-BCB composite with 7.5 vol% Al_2O_3-NPLs measured at 1 kHz and at 150 °C, respectively.

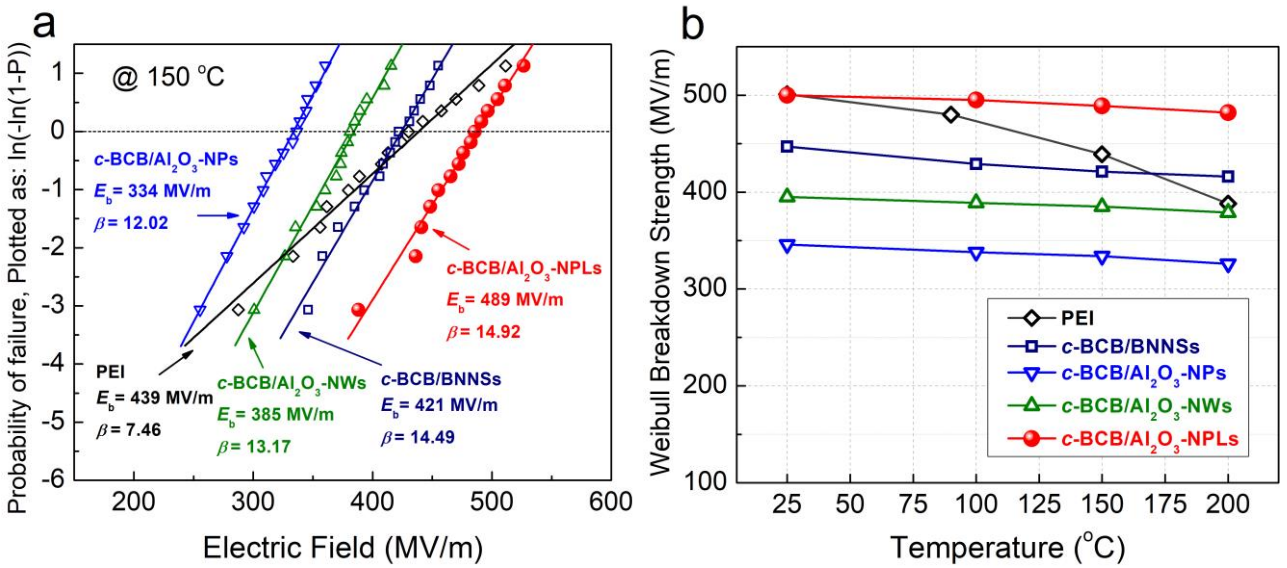

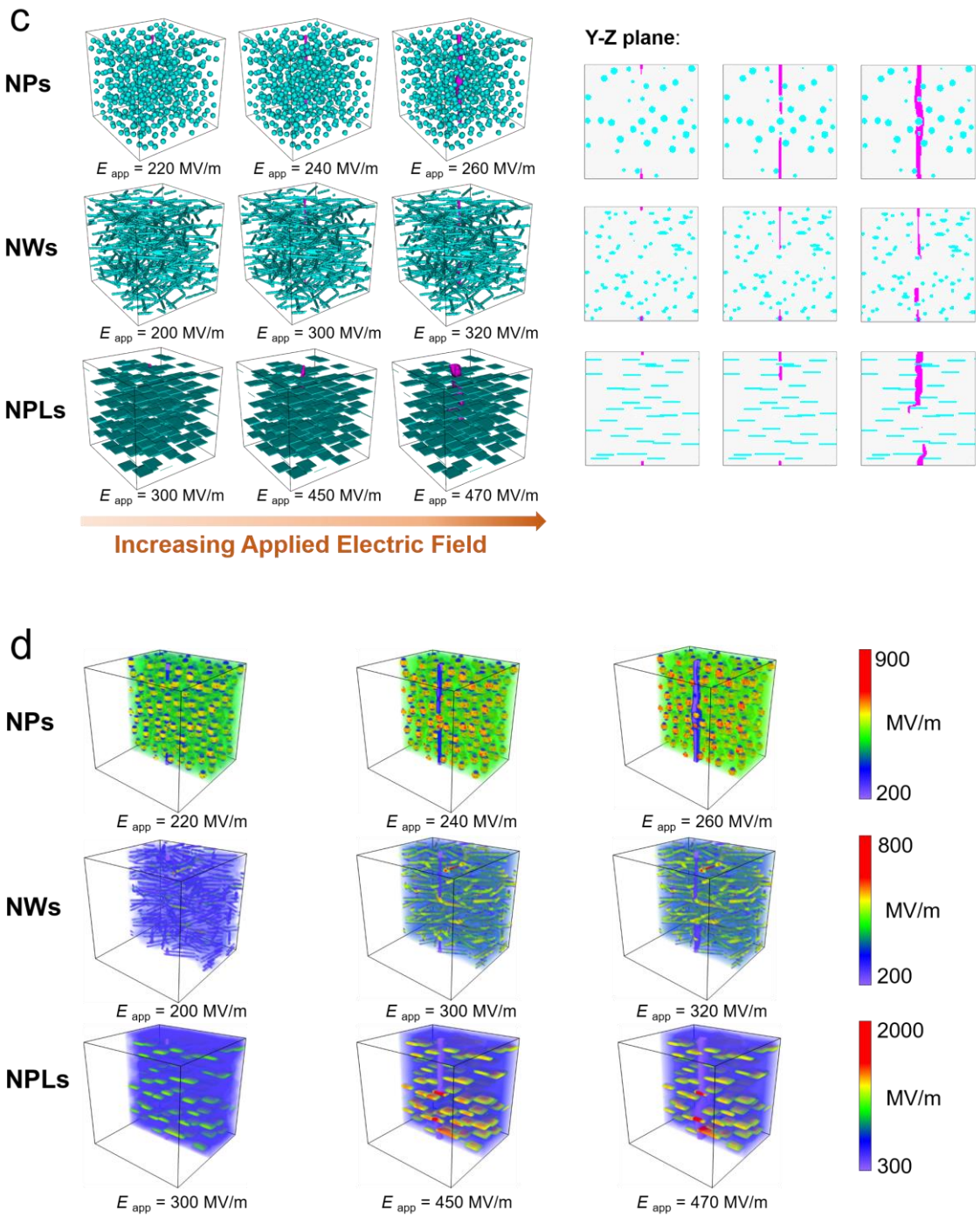

Figure 2. a) Weibull statistic of dielectric breakdown strength of PEI and the nanocomposites at 150 °C. **b)** Temperature-dependent Weibull breakdown strength of PEI and the nanocomposites at 150 °C. **c)** The predicted breakdown path evolution and **d)** the corresponding electric field distribution computed by phase-field simulations of the *c*-BCB nanocomposites with 7.5 vol% Al_2O_3 NPs, NWs and NPLs at 150 °C and varied applied electric fields.

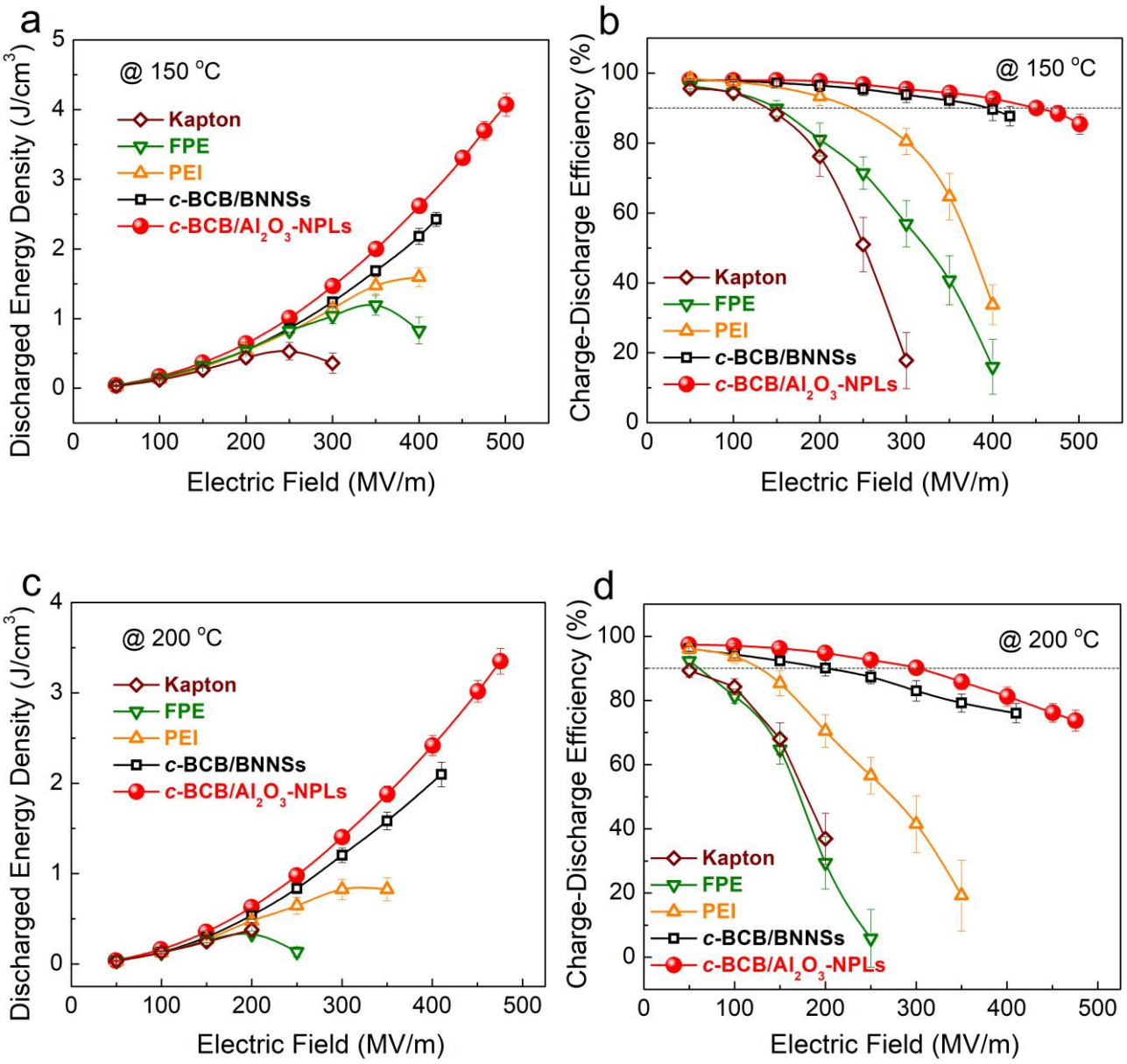

Figure 3. Discharged energy density and charge-discharge efficiency of high-temperature dielectric polymers and the *c*-BCB nanocomposites measured at **a, b)** 150 °C and **c, d)** 200 °C.

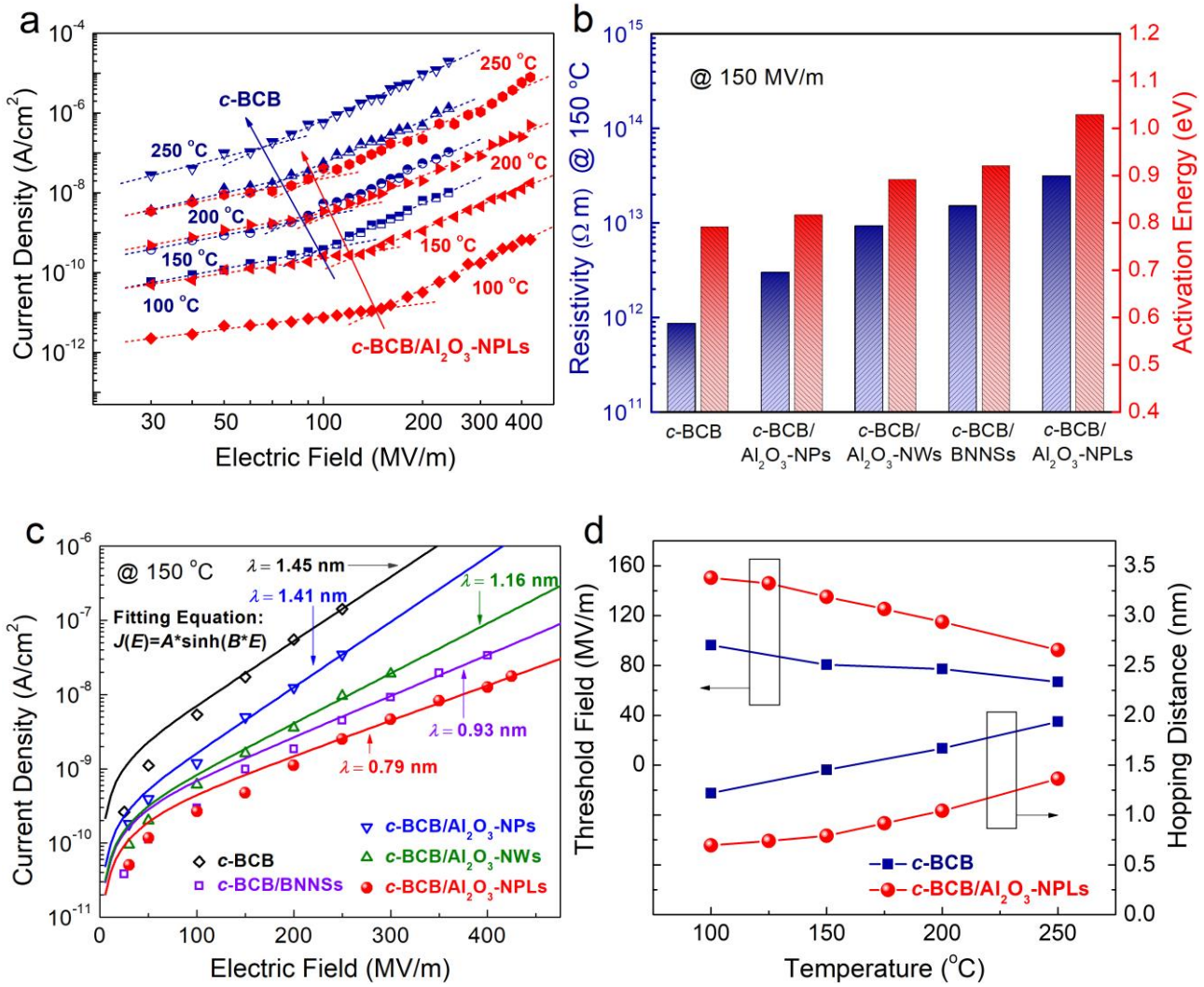

Figure 4. a) Leakage current density of *c*-BCB and the *c*-BCB nanocomposite with 7.5 vol% Al_2O_3-NPLs at evaluated temperatures as a function of electric field. **b)** Comparsion of the electrical resistivity at 150 °C and the activation energy calculated from an Arrhenius relationship at 150 MV/m of *c*-BCB and the *c*-BCB nanocomposites with 10 vol% BNNSs and 7.5 vol% Al_2O_3 NPs, NWs and NPLs. **c)** Leakage current density of *c*-BCB and the *c*-BCB nanocomposites as a function of electric field at 150 °C. Solid curves represent fit to hyperbolic sine. **d)** Temperature-dependent thershold field and hopping distance of *c*-BCB and the *c*-BCB nanocomposite with 7.5 vol% Al_2O_3-NPLs.